An Open Boundary Condition for Models of Thermals

ROBERT A. PEARSON AND JOHN L. McGREGOR[1]

Geophysical Fluid Dynamics Laboratory, Monash University, Clayton, Victoria, 3168, Australia

(Manuscript received 25 April 1975, in revised form 9 October 1975)

ABSTRACT

Numerical models of thermals usually introduce a closed box within which convection occurs. A boundary condition which allows inflow and outflow through the edges of the computational domain is discussed. The results of numerical experiments using this boundary condition are then compared and contrasted with those obtained when a rigid boundary is assumed. It is found that the flow development is especially sensitive to the choice of the upper boundary condition even before warm fluid reaches the top of the computational domain.

1. Introduction

Two- and three-dimensional numerical models of clouds usually assume that the flow is generated by a parcel of hot or humid air present in the atmosphere. The surrounding air is usually taken to be at rest although an overall shear flow may be introduced. The equations of motion are numerically integrated and the development of the cloud is followed (e.g., Lilly, 1962; Ogura, 1963; Daley and Merilees, 1971; Clark, 1973). An alternative approach is to model clouds in the laboratory (e.g., Richards, 1963) where, as in the atmosphere, the bubble of hot air is usually much smaller than the "container." In the numerical model the restrictions of computer storage capacity and computational time require a domain that is not much larger than the region of hot air (Fig. 1). If this smaller, numerically modeled region is to produce realistic results, the constraints at the computational boundaries should be consistent with the large-flow situation.

In some numerical models of other geophysical fluid flows "open" boundary conditions have been derived. These allow a small computational region without significantly influencing the interior flow. Although such formulations depend on the particular model, surface gravity waves can be allowed to pass through a computational boundary (Vastano and Reid, 1967). Dispersive waves such as internal waves can also pass through a suitably defined boundary (Pearson, 1974). In a mesoscale atmospheric model it is appropriate to allow vorticity to be advected through the boundary (Shapiro and O'Brien, 1970). Thus for a numerical model of a cloud the correct boundary conditions will depend on the ambient conditions. A stable environment will require the dispersive wave formulation at the boundary while an overall shear flow will require a more complicated boundary condition. This paper considers boundary conditions appropriate to the simplest situation.

The earliest cloud models consider dry air with no mean environmental potential temperature variations. If the model coordinates are fixed in space, the convection is assumed to occur within a box which has rigid edges. For such models all the flow is restricted to the interior and the hot air eventually reaches the top (Fig. 1).

If an asymptotic shape-preserving thermal is modeled, a moving expanding coordinate system can be used (Lilly, 1964; Fox, 1972). The outer edge of this system is also assumed to be far enough away from the developing thermal that the boundary does not influence the solution. These expanding boundaries are assumed to be rigid throughout the development of the flow

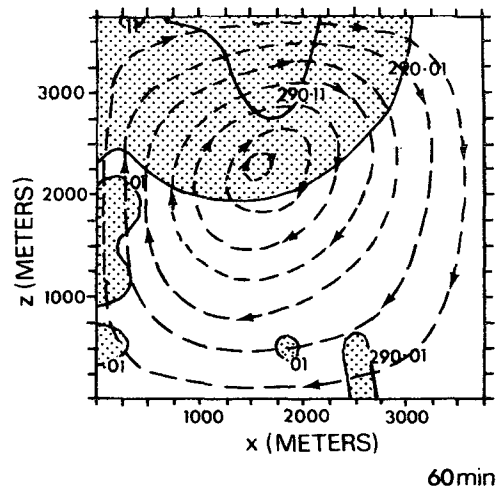

FIG. 1. Streamfunction and temperature field from Lilly (1962).

[1] Present affiliation: Australian Numerical Meteorology Research Center, Melbourne, Victoria, 3001, Australia.

field. Lilly (1964) subsequently compares the streamfunction obtained from the steady-state vorticity field and open boundary conditions with that obtained using the closed boundary. He concludes that the differences are not significant. However his argument does not imply that the steady-state vorticity field would have been similar had open boundary conditions been used.

2. The basic model

The air is dry and the Boussinesq approximation is assumed to be valid (Dutton and Fichtl, 1969). All flow is considered to be generated by convection in a constant density environment. The initial perturbation, and all subsequent flow, is to be two-dimensional in the x, z plane. With the introduction of a streamfunction ψ and vorticity ζ defined by

$$u=\frac{\partial\psi}{\partial z},\quad w=-\frac{\partial\psi}{\partial x},\quad \zeta=\frac{\partial u}{\partial z}-\frac{\partial w}{\partial x}=\nabla^2\psi,$$

the equations of motion can be written as

$$\frac{\partial\zeta}{\partial t}=J(\psi,\zeta)-\beta g\frac{\partial\theta'}{\partial x}+\nu\nabla^2\zeta,$$

$$\frac{\partial\theta'}{\partial t}=J(\psi,\theta')+\kappa\nabla^2\theta',$$

where θ' is the deviation of potential temperature from its initial constant value, ν is a coefficient of "eddy" viscosity, and κ is the coefficient of thermal "eddy" conductivity. For simplicity the coefficients ν and κ are assumed to be constant.

Initially, the fluid is assumed to be at rest with a small temperature excess in a limited region. This temperature perturbation is of the same form as that of Soong and Ogura (1973) and will be written as

$$\theta'(x,z)=\begin{cases}\theta_m\left[1-\left(\dfrac{x}{x_d}\right)^2\right]\left[1-\left(\dfrac{z-z_m}{z_d}\right)^2\right], \\ \qquad -x_d\leqslant x\leqslant x_d,\ z_m-z_d\leqslant z\leqslant z_m+z_d, \\ 0, \quad \text{otherwise.}\end{cases}$$

From this symmetry at the z axis we have $\psi(0,z)=0$ and $\zeta(0,z)=0$ for all time.

The flow is considered to extend unbounded in the positive z half-plane. The computational domain for the numerical model is defined by $0\leqslant x\leqslant L$ and $0\leqslant z\leqslant H$. At the bottom ($z=0$), a rigid ($w=0$), free-slip, insulating ($\partial\theta'/\partial z=0$) boundary is applied. This restriction can be relaxed to allow a completely unbounded domain.

The governing equations are integrated via a finite-difference analogue in which the temperature, vorticity and streamfunction are each defined at the grid-points $j\Delta x$, $k\Delta z$. Second-order, centered finite-difference methods are used for the linear terms. The nonlinear terms in the equations are represented by Arakawa's Jacobian (1966). This is a quadratically conservative finite-difference scheme but may give large phase errors in the advective terms (Orszag, 1971).

The Nyström (or "leap frog") technique is applied to the time integration. For stability the diffusion terms are evaluated at the lagged time step. The linear stability of the diffusion terms requires

$$\Delta t\leqslant\frac{(\Delta x)^2}{16\kappa}\quad\text{if}\quad \Delta x=\Delta z.$$

3. General behavior

Initially there is no vorticity or flow inside the fluid, although the specified initial temperature gradients will generate vorticity. The resulting flow field advects the overall temperature excess upward. The conduction of heat decreases the maximum value of the temperature perturbation and spreads it over a larger area of the fluid. Since the temperature field remains symmetric about the z axis, the vorticity is skew-symmetric. Reduction in the circulation can occur through viscous dissipation at the z axis and on the $z=0$ boundary.

4. Derivation of the boundary condition

The streamfunction in fixed coordinates for a single vortex pair of strength κ_i with center $\pm x_i$, z_i is given by

$$\psi_i(x,z)=\frac{\kappa_i}{4\pi}\log\left[\frac{(x-x_i)^2+(z-z_i)^2}{(x+x_i)^2+(z-z_i)^2}\right]. \tag{4.1}$$

(e.g., Lamb, 1932, pp. 221–222). The total streamfunction can be obtained by summing the individual contributions from all vortex pairs in the system.

In the finite-difference model a typical grid-point $(j\Delta x, k\Delta z)$ has vorticity ζ_{jk} which is taken to represent the average over an area $\Delta x\Delta z$. The elemental circulation for each grid-point coupled with its negative image at $-j\Delta x$, $k\Delta z$ is thus $\kappa_{jk}=\zeta_{jk}\Delta x\Delta z$. The contribution to the streamfunction from each vortex pair is then

$$\psi_{jk}(x,z)=\frac{\zeta_{jk}\Delta x\Delta z}{4\pi}\log\left[\frac{(x-x_j)^2+(z-z_k)^2}{(x+x_j)^2+(z-z_k)^2}\right]. \tag{4.2}$$

For our purposes we can assume that x, z does not coincide with x_j, z_k, although it is straightforward to resolve the apparent singularity in such cases.

To satisfy the constraint of zero normal flow through the bottom boundary it is necessary to impose negative image vorticity below $z=0$. The contribution to the streamfunction from an image vortex pair below the bottom is numerically the same as $-\psi_{jk}(x,-z)$.

Compatible with all flow being generated by convection inside the computational domain, the present model requires the vorticity to be exponentially small

for all $x \geqslant L$ or $z \geqslant H$. Thus the total streamfunction at any point x, z is given by

$$\psi(x,z)=\sum_{j=0}^{(L/\Delta x)-1}\sum_{k=0}^{(H/\Delta z)-1}[\psi_{jk}(x,z)-\psi_{jk}(x,-z)]. \quad (4.3)$$

This expression serves as a boundary condition for the sides of the computational domain. Interior values of the streamfunction are subsequently obtained by inverting a Poisson equation ($\zeta=\nabla^2\psi$) using standard numerical methods.

Eq. (4.3) requires a double summation for each point on the boundary, and hence a very large amount of computer time. A number of simplifications are therefore introduced.

5. Simplified boundary conditions

(*a*) Consider polar coordinates r, ϕ corresponding to the previous x, z coordinate system, with $x=r\sin\phi$, $z=r\cos\phi$. Now from Kellogg (1929, p. 145), we have for $r>r_i$

$$-\tfrac{1}{2}\log[(x-x_i)^2+(z-z_i)^2]$$
$$=\log\frac{1}{r}+\cos(\phi-\phi_i)\frac{r_i}{r}+\tfrac{1}{2}\cos 2(\phi-\phi_i)\frac{r_i^2}{r^2}$$
$$+\tfrac{1}{3}\cos 3(\phi-\phi_i)\frac{r_i^3}{r^3}+\cdots, \quad (5.1)$$

with a similar formula for $r<r_i$. Substituting (5.1) and a similar expansion with $x+x_i$ into (4.1) gives for $r>r_i$

$$\psi_i(x,z)=\frac{-\kappa_i}{\pi}\left[\cos\phi\cos\phi_i\frac{r_i}{r}+\tfrac{1}{2}\sin\phi\sin\phi_i\frac{r_i^2}{r^2}\right.$$
$$\left.+\tfrac{1}{3}\cos 3\phi\cos 3\phi_i\frac{r_i^3}{r^3}+\cdots\right]. \quad (5.2)$$

In the Cartesian coordinate system for an upper vortex pair

$$\psi_{jk}(x,z)=-\frac{x_j\zeta_{jk}\Delta x\Delta z}{\pi r^2}\left[1+\frac{2zz_k}{r^2}+\frac{1}{3r^4}(x^2-3z^2)(x_j^2-3z_k^2)\right.$$
$$+\frac{4zz_k}{r^6}(x^2-z^2)(x_j^2-z_k^2)+\frac{1}{5r^8}(x^4-10x^2z^2+5z^4)$$
$$\left.\times(x_j^4-10x_j^2z_k^2+5z_k^4)+\cdots\right]. \quad (5.3)$$

As many terms as necessary can be used in this expansion. In the form used above there are errors of order $(r_i/r)^6$.

The advantage of this expansion is that when it is substituted into (4.3) the sum of each of the five moments over all points within the domain of integration are easily calculated, e.g., $\sum\sum x_j\zeta_{jk}$, $\sum\sum x_jz_k\zeta_{jk}$.[2] As these same moments can be used for all points on the boundary only five double summations are required.

(*b*) Far from the center of vorticity the streamfunction pattern will resemble that of a line vortex centered at some point $(\bar{x},\bar{z})$. The traditional definition (Lamb, 1932, p. 220) gives

$$\bar{x}=\frac{\sum\sum x_j\zeta_{jk}\Delta x\Delta z}{\sum\sum\zeta_{jk}\Delta x\Delta z}, \quad (5.4)$$

$$\bar{z}=\frac{\sum\sum z_k\zeta_{jk}\Delta x\Delta z}{\sum\sum\zeta_{jk}\Delta x\Delta z}, \quad (5.5)$$

where the total circulation $\bar{\kappa}$ is given by

$$\bar{\kappa}=\sum\sum\zeta_{jk}\Delta x\Delta z. \quad (5.6)$$

Substitution into (4.2) and (4.3) gives

$$\psi(x,y)=\frac{\bar{\kappa}}{4\pi}\log\left[\frac{(x-\bar{x})^2+(z-\bar{z})^2}{(x+\bar{x})^2+(z-\bar{z})^2}\right]$$
$$\times\left[\frac{(x+\bar{x})^2+(z+\bar{z})^2}{(x-\bar{x})^2+(z+\bar{z})^2}\right]. \quad (5.7)$$

(*c*) The second term of (5.3) suggests that the mean height of the vortex should instead be defined by

$$\bar{z}=\frac{\sum\sum x_jz_k\zeta_{jk}\Delta x\Delta z}{\sum\sum x_j\zeta_{jk}\Delta x\Delta z}, \quad (5.8)$$

to give the streamfunction more accurately at large distances. For the experiments discussed in this paper no significant difference was found between definitions (5.5) and (5.8) for the mean height.

(*d*) In (5.1) the polar coordinate system has been centered at the origin. However, the smaller r_i is in relation to r, the faster will the series converge. The r_i can be decreased by setting the center of the polar coordinate system above the origin at $(0,\bar{z})$ and defining the distance r relative to this center.

6. Consistency of the boundary conditions

In deriving the boundary condition it has been assumed that excepting image vorticity, there is no vorticity outside the computational domain. As a horizontal temperature gradient will generate vorticity this requires that there is no temperature perturbation outside the domain. The boundary condition on the streamfunction is therefore only valid either until the temperature or the vorticity perturbation reaches the sides or top of the domain.

In addition to values of the streamfunction, the numerical model requires values of the vorticity and

[2] In this and all subsequent double summations the limits are $0\leqslant j\leqslant L/\Delta x$, $0\leqslant k\leqslant H/\Delta z$.

temperature field at the boundaries ($x=L, z=H$). These values may be found either by fixing a value at the boundary or specifying a gradient condition. If a gradient condition is used the finite-difference analog will actually relate the value at the boundary to the internal values.

Suppose that the condition $\zeta=0$ is applied at $z=H$. Should ζ just inside the boundary become non-zero, real outflow would at some later time create non-zero vorticity at the top. This is in contradiction to the applied boundary condition.

Alternatively, assume that the gradient of temperature is forced to be zero; numerically this can be written as $T(H)=T(H-\Delta z)$. Consider the situation with inflow at the boundary but large heat conduction. The heat conduction will let the temperature at one grid-point inside the boundary be non-zero. The numerical application of the gradient condition will instantaneously set a non-zero temperature at the boundary. However that rise is only a consequence of the numerical model, not of the real flow.

Either a fixed boundary condition or a specified gradient condition can introduce errors. The boundary conditions will be consistent while the vorticity and temperature perturbations remain completely inside a domain of size $L-\Delta x$, $H-\Delta z$.

In some preliminary experiments, the temperature at the boundary was fixed. It was found that a zero gradient condition gave better results near the boundary. This was the boundary condition used in the experiments discussed below. For the vorticity, values at the boundary are specified to be zero.

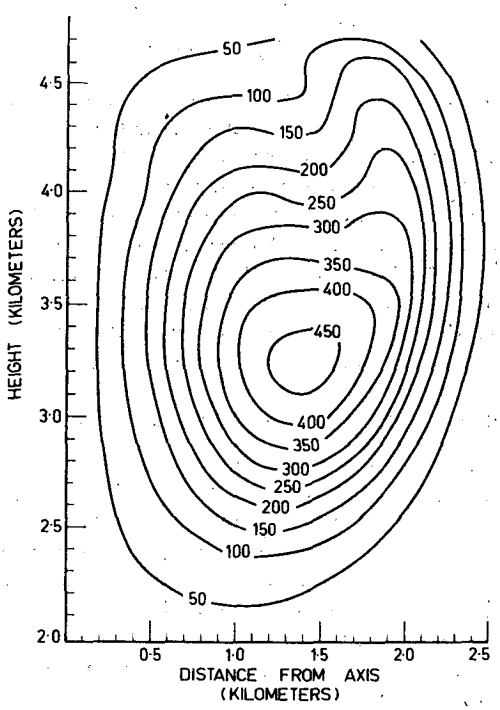

FIG. 2. Vorticity field after 60 min with contours from 0 to 4.5×10^{-3} s^{-1} at intervals of 5×10^{-4} s^{-1}. Data scaled by 10^5. Initial conditions, $\theta_m=1$ K, $x_d=0.5$ km, $z_d=0.3$ km, $z_m=0.4$ km. The computational domain has height 4.8 km and width 3.2 km with boundary conditions given by the simplest open form equations (5.4)–(5.7).

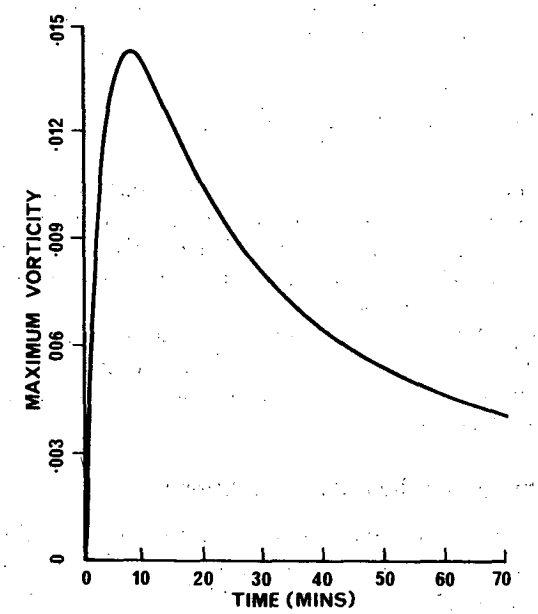

FIG. 3. Maximum vorticity (s^{-1}) as a function of time. Initial conditions as in Fig. 2.

7. Results

To evaluate the effects of the various boundary conditions and domain sizes, a number of numerical experiments were performed. The first set of experi-

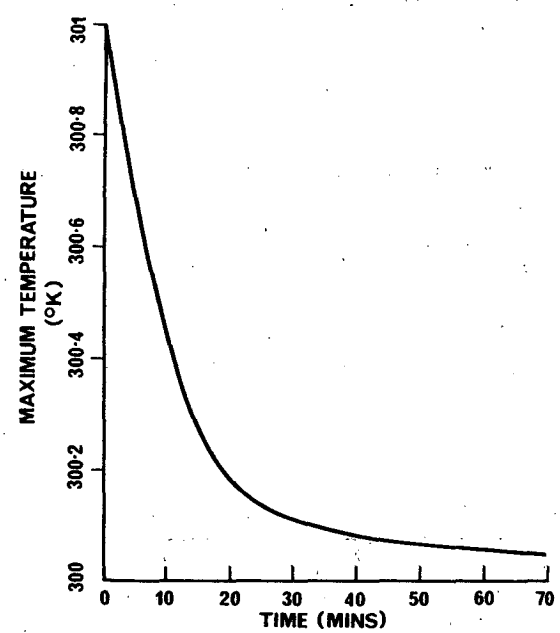

FIG. 4. Maximum temperature as a function of time. Initial conditions as in Fig. 2.

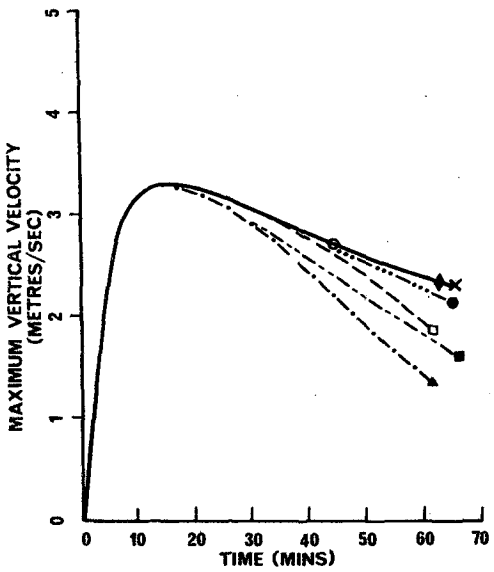

FIG. 5. Maximum vertical velocity as a function of time for the different boundary conditions. Initial conditions as in Fig. 2.

——×—— Eqs. (5.4)–(5.7) in a domain 9.6 km by 6.4 km
·····♦····· Eq. (4.3) in a domain 4.8 km by 3.2 km
– – – –○– – – – variation 5(*d*) of Eq. (5.3)
···—···● using mean vortex center equation (5.7)
— — — —■— — — — closed box 4.8 km by 3.2 km
–·–·–·–·–▲–·–·–·–·– closed box 4.0 km by 3.2 km
– – – –□– – – – using mean vortex center equation (5.7) in a domain 4.0 km by 3.2 km.

ments has an initial maximum temperature $\theta_m = 1$ K, $\nu = \kappa = 50$ m^2 s^{-1}, $\Delta x = 100$ m, $\Delta z = 100$ m, $\Delta t = 10$ s, $x_d = 500$ m, $z_d = 300$ m, $z_m = 400$ m. Boundary conditions

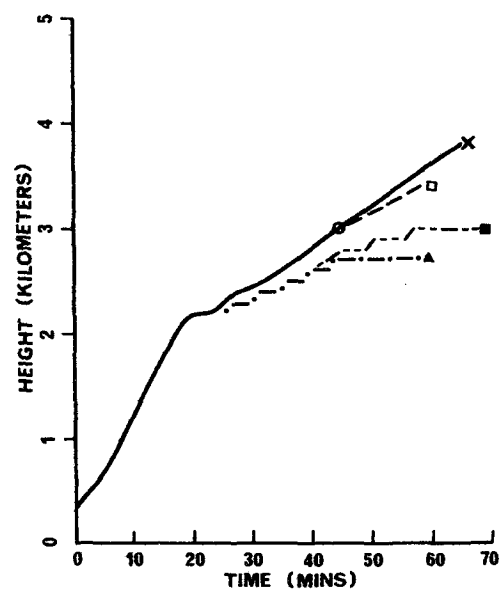

FIG. 6. Height of the maximum temperature as a function of time. Initial conditions and various boundary conditions as in Fig. 5. Eqs. (5.4) and (5.7) give the same curve as with the largest domain.

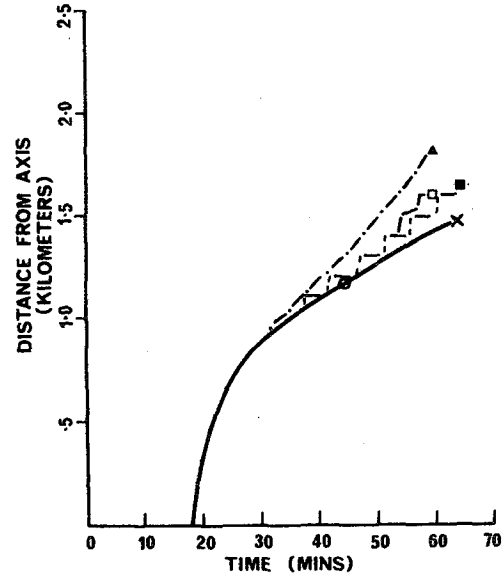

FIG. 7. Distance from the axis of the maximum temperature as a function of time. Initial conditions and various boundary conditions as in Fig. 5. Eq. (4.3) gives the same curve as the largest domain.

(5.4)–(5.7) were used for three sizes of computational domain: height 9.6 km by width 6.4 km, 4.8 km by 3.2 km, and 4.0 km by 3.2 km. A closed boundary was subsequently used for two runs with the smaller domains. An accurate calculation was performed for the intermediate size domain using (4.3) summed over the vorticity contributions from each grid point; the simplified conditions 5(*b*) and 5(*d*) were also run for this domain.

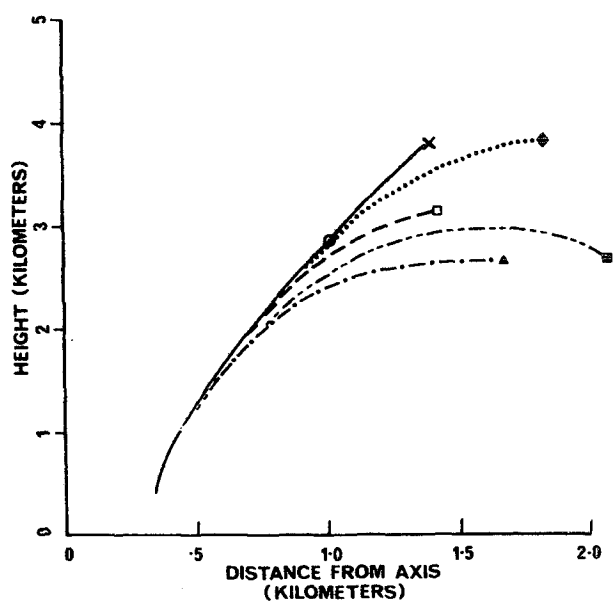

FIG. 8. Path of the average center of circulation for the cases considered in Fig. 5. Results using (5.5) and (5.8) do not differ significantly.

These initial conditions produce a vorticity field which decays radially from a maximum value (Fig. 2). The value of the vorticity at the center, and the maximum value of the temperature are the only quantities unaffected by the choice of boundary condition (Figs. 3 and 4).

The rigid upper boundary reduces the maximum velocity obtained inside the domain (Fig. 5). In comparison to the open domain the closed box gives a lower average vertical velocity of the moving "bubble" of fluid. This motion is demonstrated by the height of the maximum temperature field (Fig. 6) and the variation in the potential energy (Fig. 7). As well as decreasing the vertical speed of the "bubble" the rigid lid forces it to move further away from the z axis (Figs. 8 and 9). The differences in the results between the closed box and the largest domain begin after about 25 min of model time. At this stage the bubble is well below the top of the domain with the center at approximately (0.75, 2). The fields continue to diverge as time increases (Fig. 10).

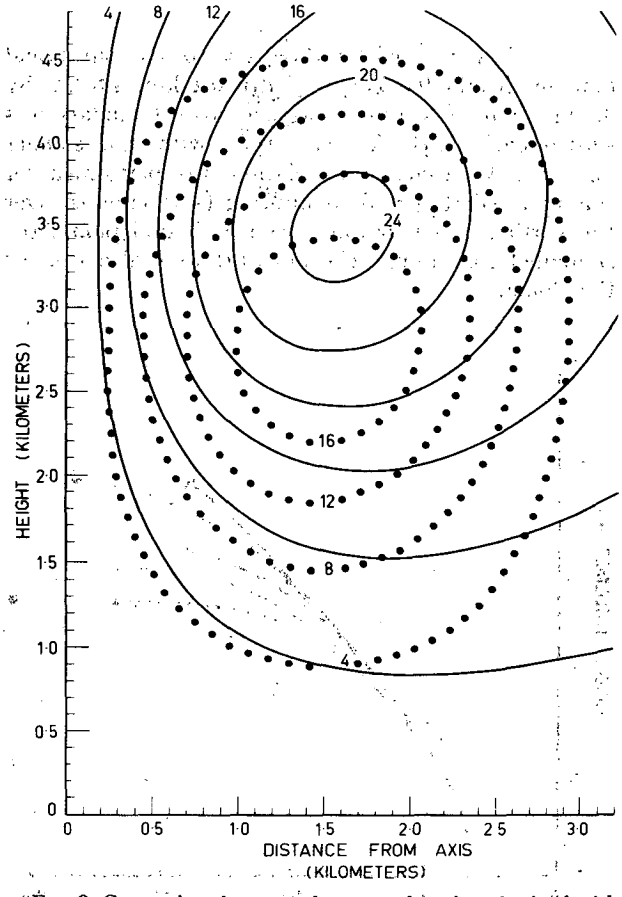

FIG. 9. Comparison between the streamfunction obtained with the largest domain (solid lines) and those with a closed box 4.8 km by 3.2 km (dotted lines). All contours are negative. Contours from 0 to -2400 m^2 s^{-1} at intervals of -400 m^2 s^{-1}. Data scaled by 10^{-2} m^2 s^{-1}.

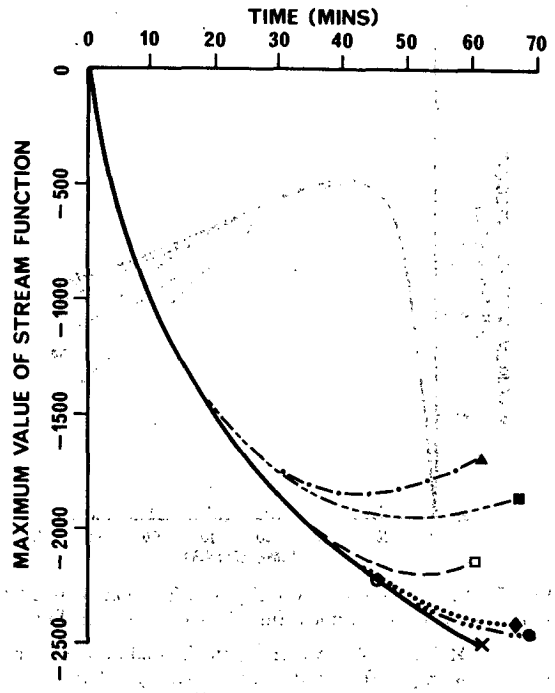

FIG. 10. Maximum value of the streamfunction (m^2 s^{-1}), as a function of time for the cases considered in Fig. 5.

The different forms of open boundary condition show values close to those obtained with the largest domain. The time over which the open condition is consistent can be found by observing the behavior of the temperature and vorticity fields, or by calculation of the heat contained inside a standardized region 3.1 km wide and 4.7 km high. This is one grid-point smaller in dimension than the total computational domain of the intermediate

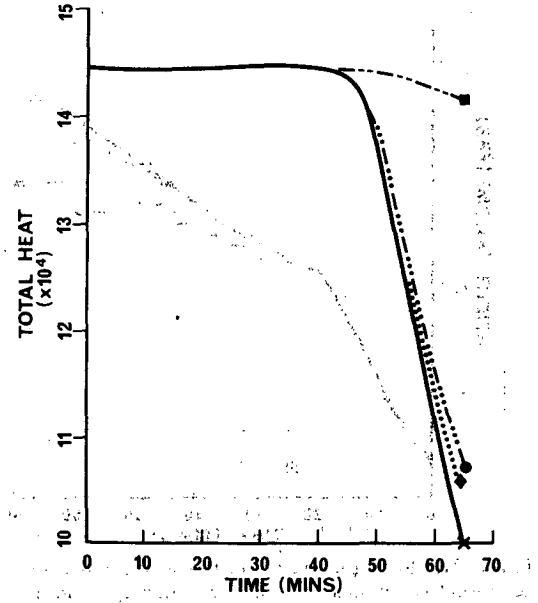

FIG. 11. Heat contained (K m^2) in a region 4.7 km by 3.1 km.

box. In this set of experiments the boundary condition is inconsistent after about 45 min. This is the same time at which variation 5(d) of the boundary condition becomes invalid with $r_i > r$. However, in this test the results for the various forms of open domain continue to agree favorably with the large domain even after vorticity and heat have been lost from the domain (Fig. 11). After 60 min the simplest open boundary condition gives results very similar to those obtained from the largest domain (Fig. 12).

The second set of numerical experiments has an initial temperature maximum $\theta_m = 0.5$ K, $x_d = 800$ m, $z_d = 400$ m, $z_m = 500$ m, $\nu = \kappa = 10$ m^2 s^{-2}. This develops finally into separate bubbles with two regions of excess temperature. The associated vorticity field has both positive and negative regions (Fig. 13). The maximum value of the temperature is very similar in both of these regions. The paths of the off-axis maximum, for the open domains, are unaffected by the form of the boundary condition.

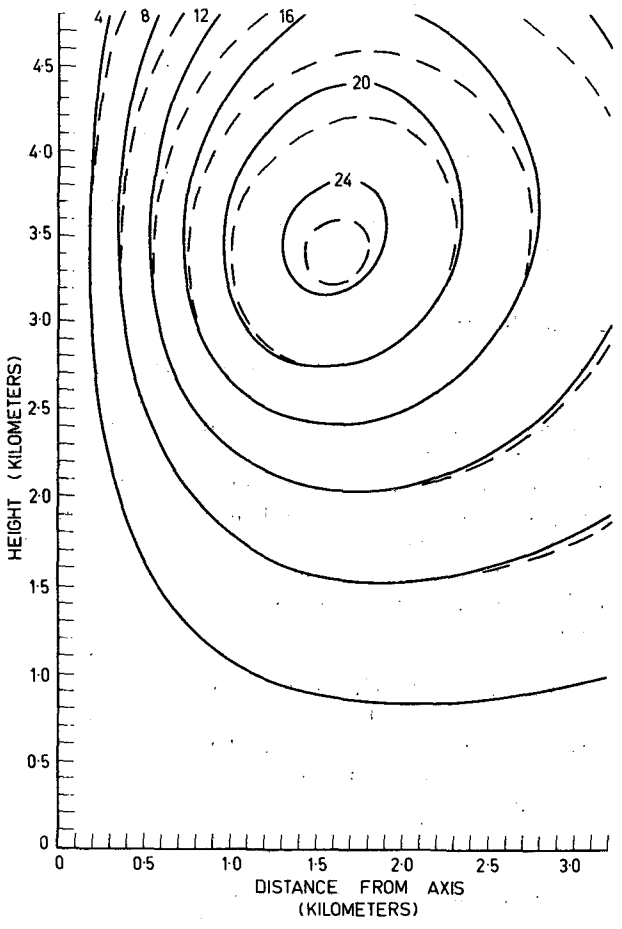

FIG. 12. Comparison between the streamfunction fields found using the largest domain (solid lines) and those obtained using Eq. (5.7) in a domain 4.8 km by 3.2 km (dashed lines). All contours are negative. Contours from 0 to -2400 m^2 s^{-1} at intervals of -400 m^2 s^{-1}. Data scaled by 10^{-2} m^2 s^{-1}.

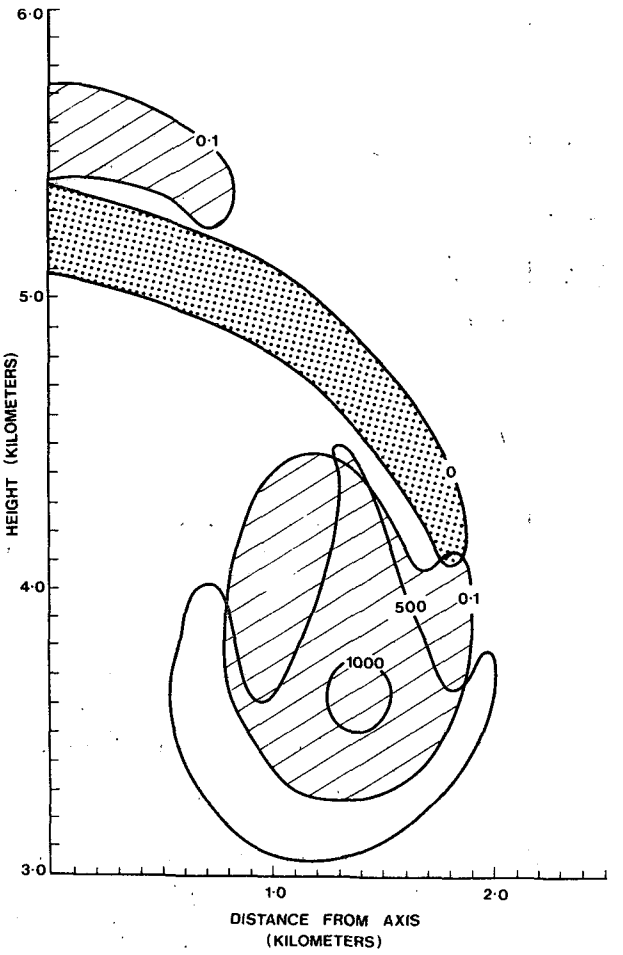

FIG. 13. Temperature (cross-hatched area) and vorticity after 60 min (negative vorticity is dotted). $\theta_m = 0.5$ K, $x_d = 0.8$ km, $z_d = 0.4$ km, $\nu = \kappa = 10$ m^2 s^{-1}. Contours of excess temperature in K. Vorticity contoured from zero to 1×10^{-2} s^{-1}, at intervals of 5×10^{-3} s^{-1}. Data scaled by 10^5 s^{-1}.

Once again the maximum values of both temperature and vorticity are not significantly affected by the size of the domain. The maximum velocity (Fig. 14) and motion of the "bubble" (Fig. 15) show the same behavior as that in the previous set of experiments. The differences between the various boundary conditions begin when the mean center of the bubble is at approximately (0.5, 1).

For this second set of experiments the various open boundary conditions, while consistent, give identical results to those obtained with the larger domain. As expected, they begin to diverge when the flow field does not satisfy the consistency requirement. However, the simplest form continues to give reasonable results (Fig. 16) even though a significant amount of heat has passed through the top of the domain.

For both the above experiments the open boundary condition became inconsistent at approximately twice the model time at which the rigid boundary began to

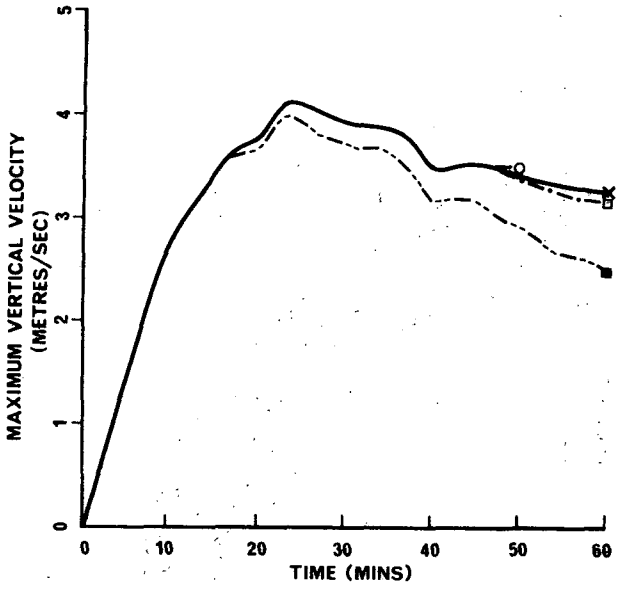

FIG. 14. Maximum vertical velocity as a function of time. Initial conditions as in Fig. 13.

——X Eqs. (5.4)–(5.7) in a domain 9.6 km by 6.4 km
·····△ Eq. (4.2) in a domain 4.8 km by 3.2 km
-·-·-·-□ Eqs. (5.4)–(5.7) in a domain 4.8 km by 3.2 km
- - - - -○ variation 5(*d*) of Eq. (5.3) in a domain 4.8 km by 3.2 km
— - - -■ rigid boundary on a box 4.8 km by 3.3 km.

affect the solution. The number of points used was only a quarter of those needed for the largest domain. As the simplest boundary conditions yield good results the amount of computer time and space needed is considerably reduced.

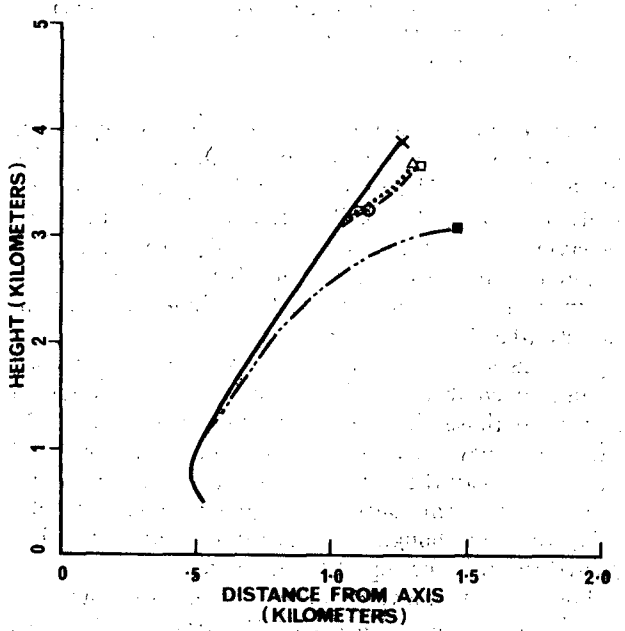

FIG. 15. Path of the mean center of circulation. Initial conditions as in Fig. 13.

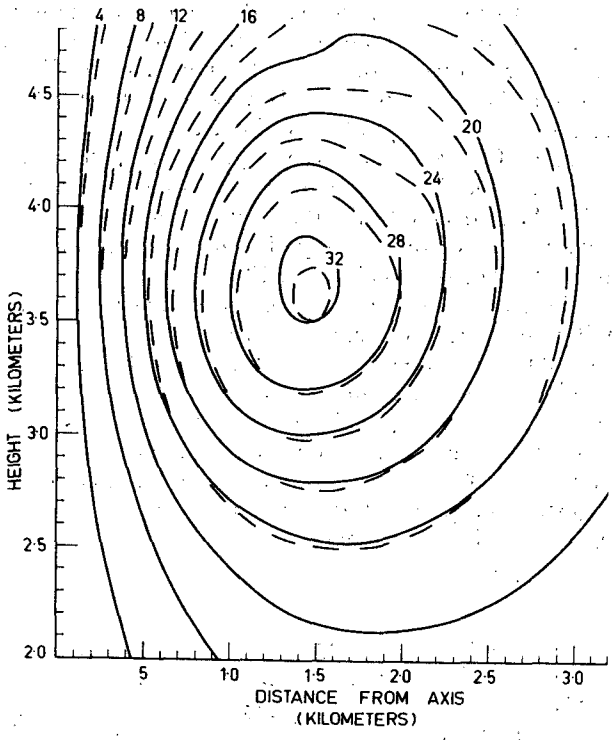

FIG. 16. Comparison between streamfunction fields after 60 min. Initial conditions as in Fig. 13. Values obtained from a domain 9.6 km by 6.4 km (solid lines) with Eqs. (5.4) to (5.7) and a domain 4.8 km by 3.2 km with Eqs. (5.4) to (5.7) (dashed lines). All contour lines are negative. Contours from 0 to -3200 m^2 s^{-1} at intervals of -400 m^2 s^{-1}. Data scaled by 10^{-2} m^2 s^{-1}.

8. Conclusion

For convection in a neutral environment it has been shown that the form of the boundary condition will influence the behavior of the solution well before any temperature perturbation reaches the top of the computational region. The simplest open boundary condition gives accurate results as long as all temperature and vorticity remain inside the domain. At later model times good agreement is found, even though the flow field is theoretically inconsistent with the derived boundary condition.

Acknowledgments. This work was done while the first author was supported by a grant from the Australian Research Grants Committee. The authors would like to thank J. R. Crawford for his help in the programming.

REFERENCES

Arakawa, A., 1966: Computational design for long-term numerical integration of the equations of fluid motion: Two-dimensional incompressible flow. Part 1. *J. Comput. Phys.*, **1**, 119–143.

Clark, T. L., 1973: Numerical modeling of the dynamics and microphysics of warm cumulus convection. *J. Atmos. Sci.*, **30**, 857–878.

Daley, R., and P. Merilees, 1971: A spectral model of bubble convection. *J. Atmos. Sci.*, **28**, 933–943.

Dutton, J. A., and G. H. Fichtl, 1969: Approximate equations of motion for gases and liquids. *J. Atmos. Sci.*, **26**, 241–254.

Fox, D. G., 1972: Numerical simulation of three-dimensional, shape-preserving convective elements. *J. Atmos. Sci.*, **29**, 322–341.

Kellogg, O. D., 1929: *Foundations of Potential Theory*. Frederick Ungar Publishing Company, 384 pp.

Lamb, H., 1932: *Hydrodynamics*, 6th ed. Cambridge University Press, 738 pp.

Lilly, D. K., 1962: On the numerical simulation of buoyant convection. *Tellus*, **14**, 148–172.

——, 1964: Numerical solutions for the shape-preserving two-dimensional thermal convection element. *J. Atmos. Sci.*, **21**, 83–98.

Ogura, Y., 1963: The evolution of a moist convective element in a shallow, conditionally unstable atmosphere: A numerical calculation. *J. Atmos. Sci.*, **20**, 407–424.

Orszag, S. A., 1971: Numerical simulation of incompressible flows within simple boundaries: Accuracy. *J. Fluid Mech.*, **49**, 75–112.

Pearson, R. A., 1974: Consistent boundary conditions for numerical models of systems that admit dispersive waves. *J. Atmos. Sci.*, **31**, 1481–1489.

Richards, J. M., 1963: Experiments on the motion of isolated cylindrical thermals through unstratified surroundings. *Intern. J. Air. Water Pollution*, **17**, 17–34.

Shapiro, M. A., and J. J. O'Brien, 1970: Boundary conditions for fine-mesh limited-area forecasts. *J. Appl. Meteor.*, **9**, 345–349.

Soong, S-T., and Y. Ogura, 1973: A comparison between axisymmetric and slab-symmetric cumulus cloud models. *J. Atmos. Sci.*, **30**, 879–893.

Vastano, A. C., and R. O. Reid, 1967: Tsunami response for islands: Verification of a numerical procedure. *J. Marine Res.*, **25**, 129–139.